Structure and basal twinning of topological insulator Bi_{2}Se_{3} grown by MBE onto crystalline Y_{3}Fe_{5}O_{12}

Danielle Reifsnyder Hickey, Javad G. Azadani, Anthony R. Richardella, James C. Kally, Joon Sue Lee, Houchen Chang, Tao Liu, Mingzhong Wu, Nitin Samarth, Tony Low, and K. Andre Mkhoyan

Phys. Rev. Materials **3**, 061201 — Published 25 June 2019

DOI: 10.1103/PhysRevMaterials.3.061201

Structure and basal twinning of topological insulator Bi_2Se_3 grown by MBE onto crystalline $Y_3Fe_5O_{12}$

Danielle Reifsnyder Hickey,[1,2] Javad G. Azadani,[3] Anthony R. Richardella,[4] James C. Kally,[4] Joon Sue Lee,[4,5] Houchen Chang,[6] Tao Liu,[6] Mingzhong Wu,[6] Nitin Samarth,[4] Tony Low,[3] K. Andre Mkhoyan[1]*

[1]Department of Chemical Engineering and Materials Science, University of Minnesota, Minneapolis, MN 55455

[2]Department of Materials Science and Engineering, The Pennsylvania State University, University Park, PA 16802

[3]Department of Electrical and Computer Engineering, University of Minnesota, Minneapolis, MN 55455

[4]Department of Physics, The Pennsylvania State University, University Park, PA 16802

[5]California NanoSystems Institute, University of California, Santa Barbara, CA 93106

[6]Department of Physics, Colorado State University, Fort Collins, CO 80523

*Corresponding author: mkhoyan@umn.edu

Abstract:

Whereas thin films of topological insulators grown by molecular beam epitaxy often display regular, triangular features, Bi_2Se_3 films grown onto yttrium iron garnet (YIG) display much greater disorder. Here, we present observations of various types of disorder present in these films using atomic force microscopy and scanning transmission electron microscopy. The investigation reveals the presence of an amorphous metal oxide layer between the substrate and the film, which appears to smooth out the nanometer-scale undulations in the YIG surface. It also shows the existence of quasi-ordered arrays of heavy atoms in some interfacial regions, as well as rotations and tilting between adjacent grains and basal twinning at various heights in the film. Using density functional theory, we explore the impact of these prominent basal twins on the electronic structure of the film.

Main Text:

Achieving efficient spin-to-charge and charge-to-spin conversion in topological insulators (TIs) such as Bi_2Se_3 is critical to enabling the development of next-generation spintronics [1–3]. Yet, probing these phenomena has been complicated because device geometries have included contact between the TI layer and a ferromagnetic metal, resulting in current shunting. Therefore, TIs have recently been integrated onto ferrimagnetic insulator thin films [4–6], allowing for isolation of the TI surface states.

Yttrium iron garnet ($Y_3Fe_5O_{12}$, or YIG) is a technologically interesting substrate because of its high Curie temperature of ~560 K and extremely low damping coefficient [6,7], and therefore it is a good candidate substrate for TIs. However, Bi_2Se_3 TI films grown onto YIG substrates exhibit greater disorder than analogous films grown onto traditional substrates [5,8,9]. This presents a significant challenge because the nature of the spin–momentum-locked conducting surface states in TIs is likely susceptible to any deviation from its pristine atomic structure. For example, the local structural features of the TI film, such as stacking faults, rotational twin boundaries, and strain, are shown to impact device performance [10–12].

Bi_2Se_3 and other thin-film TIs from the tetradymite crystal family are notable for being able to grow on numerous substrates with significant lattice mismatch. They typically grow *via* van der Waals epitaxy, in which there is often a dominant crystallographic relationship between the substrate and the thin film, but the tolerance for lattice parameter mismatch is higher than for traditional epitaxy. Bi_2Se_3 and its analogs have previously been grown onto the (111) plane of a number of cubic substrates (e.g., Si [13,14], InP [8,15], and GaAs [16]) and onto other substrates with hexagonal symmetry, such as graphene [17,18] and hexagonal-BN [19,20].

Here, we present structural characterization of thin films of Bi_2Se_3 grown by molecular beam epitaxy (MBE) onto crystalline YIG [5]. The YIG (~20 nm thick) was grown onto a single-crystal (111)-

oriented gadolinium gallium garnet (GGG) substrate in an ultrahigh vacuum sputtering system [7] at 25 mTorr Ar pressure. In the MBE chamber prior to Bi_2Se_3 growth, the YIG surface was cleaned *in situ* by heating to a substrate temperature of 400 °C 500 °C for an hour, before cooling the sample for the film growth. The Bi_2Se_3 films were grown according to Ref. [5], using a two-step growth sequence in which the first 2 nm were deposited at relatively low temperatures (room temperature or 200 °C) to promote film adhesion to the substrate. These layers were annealed under Se flux for 35 40 min, and then the remaining 4 nm were grown at 325 °C. The surface features of the films were studied *via* atomic force microscopy (AFM), using a DI Dimension AFM in tapping mode. The atomic structures of the MBE-grown Bi_2Se_3 thin films and the Bi_2Se_3/YIG interfaces were investigated *via* analytical scanning transmission electron microscopy (STEM), using an FEI Titan G2 60-300 aberration-corrected S/TEM equipped with a Schottky X-FEG gun [20]. Density functional theory (DFT) calculations were performed as described in Ref. [20]. Calculations were performed using the projector-augmented wave (PAW) method [21] as implemented in the Vienna *ab initio* simulation package (VASP) [22]. The exchange-correlation energy is described by the GGA using the PBE functional [23]. The Brillouin zone was sampled using 20x20x1 Γ-centered Monkhorst-Pack *k*-points mesh with spin–orbit coupling taken into consideration. van der Waals corrections were included for the atomic relaxations [24].

The AFM measurements (Fig. 1(a,b)) provide a quantitative comparison of the topography of the YIG substrate and the Bi_2Se_3 film grown onto it, showing the height variations in the substrates and TI films and highlighting structural irregularities. Unlike Bi_2Se_3 films grown onto a nearly atomically flat sapphire substrate, for which consistent terraces of several five-atom-thick quintuple layers (QLs) of Bi_2Se_3 [8,25–27] are visible, Figs. 1(a,b) show that: (i) the surface of the YIG substrate has considerable (from 0.5 nm to as large as 3.0 nm) height variations that form shallow pits, and (ii) the resulting Bi_2Se_3 film is smoother than the YIG substrate (even though pits as deep as 6.0 nm exist in a few places), but still much less regular than that grown on sapphire, both in symmetry and height. To grow the Bi_2Se_3 film with grains as large as > 200 nm onto the YIG substrate, the undulations in the substrate surface must either become infilled with amorphous precursor, stay vacant, or template the Bi_2Se_3 growth so that it conforms to the YIG surface morphology. Although YIG films grow epitaxially onto GGG with no observed defects, the interface between YIG and Bi_2Se_3 appears, upon initial inspection, to lack obvious structure and be consistent with previous independent reports [5,6]. Prior to this work, this interface has been characterized as simply an amorphous layer that is ~ 1 nm thick.

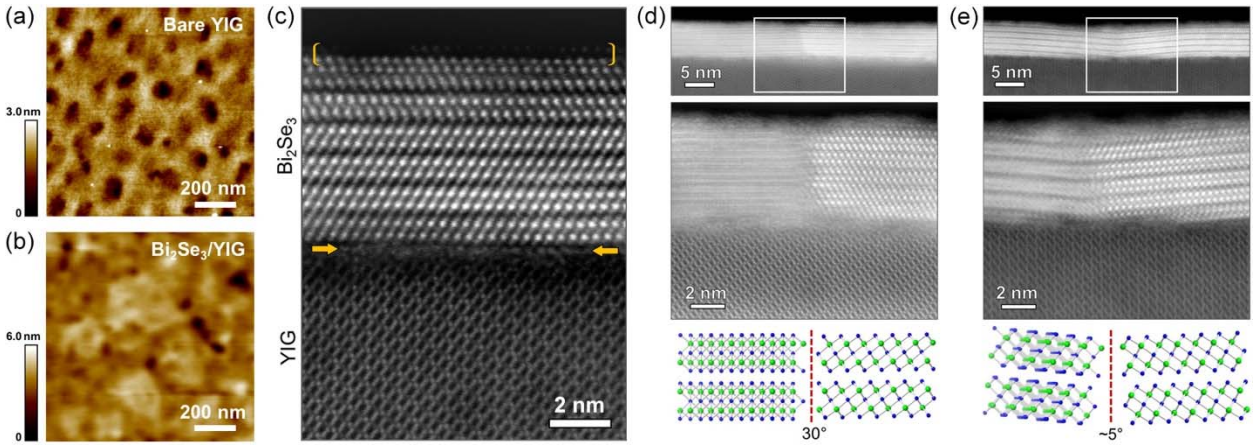

FIG. 1. AFM images of (a) a bare YIG substrate and (b) a Bi_2Se_3 film grown onto a YIG substrate. (c) Atomic-resolution cross-sectional HAADF-STEM image showing a disordered heavy-atom layer at the Bi_2Se_3/YIG interface (yellow arrows) and an extra Bi monolayer on the upper surface of the Bi_2Se_3 film (in yellow brackets). Cross-sectional HAADF-STEM images of (d) flat and (e) tilted grain boundaries, shown at low magnification with the surrounding grains and at high magnification to display the atomic structure. (d) A flat grain boundary, where two grains have 30° rotational mismatch but maintain registry in the out-of-plane direction. (e) A tilted grain boundary, around which the two grains have low-angle rotational mismatch and are tilted relative to each other and the substrate (~ 5°).

Because the YIG substrate has variation in the surface topography that impacts how the Bi_2Se_3 film is able to grow, cross-sectional STEM analysis was performed to better understand the atomic structure of the Bi_2Se_3 film. Figs. 1(c-e) show high-angle annular dark-field (HAADF)-STEM images of a cross section of the Bi_2Se_3/YIG system at different locations. In many places, the YIG substrate appears separated from the QLs of Bi_2Se_3 by a relatively large interfacial layer that is 1 □ 2 nm thick. Whereas the crystalline structures of the YIG and Bi_2Se_3 films are apparent, an ill-defined layer between the YIG and Bi_2Se_3 films is clearly visible as well. STEM-EDX elemental maps across the interface (not shown) indicate that this layer comprises a mixture of the elements Bi, Se, Y, Fe, and O, as expected, with slight enrichment in Bi and Fe. The majority of this layer appears to be amorphous, consistent with predictions based on our AFM results discussed earlier and previous observations reported in the literature [5,6]. However, in some areas, we observe several-nm-long regions containing quasi-ordered arrays of heavy atoms (see Fig. 1(c), indicated by yellow arrows). These observations indicate a coexistence of disordered and quasi-ordered interfacial regions. Although this, to the best of our knowledge, is the first report of such quasi-ordered arrays of heavy atoms at the Bi_2Se_3/YIG interface, it is not clear why they form under some Bi_2Se_3 grains but not others.

Rotations and tilting are observed between the grains in the Bi_2Se_3 film. Figs. 1(d) and (e) show examples of a 30° and a low-angle (a few degrees) grain boundary. Here, the low-angle grain boundary

also exhibits a tilt by ~ 5° off the *c*-axis. It should be noted here that low-angle and high-angle grain boundaries are common in MBE-grown TI films [12,20]. However, directly observed cases of Bi_2Se_3 film grains that are tilted off the c-axis are rare [25,28]. This tilting, which is the result of a discontinuous bottom QL at the boundary, can be a pathway for the TI film to compensate for the shallow dips and undulations on the surface of the YIG substrate.

Cross-sectional HAADF-STEM imaging reveals an additional, internal type of disorder in the grains of the Bi_2Se_3 film. Figs. 2(a-d) show basal twins observed at various locations (or heights) in the different grains of the Bi_2Se_3 film. The presence of basal twins previously has been linked to strain in TI films [29]. To evaluate the effects of the basal twins on the electronic band structure of the Bi_2Se_3 films, we performed DFT calculations. For 6-QL-thick films, the calculations indicate that the presence of a basal twin in a Bi_2Se_3 thin film opens up a band gap in the Dirac surface states (see Fig. 2(e-h)). Other more subtle changes in the band structure, including changes in the spin–momentum angle, also occur in the film as a function of the location of the basal twin in the film (see Fig. 2(e-h)). Here, calculations were performed with fixed lattice constants for the Bi_2Se_3 QLs: a = 4.11 Å and c = 54.93 Å, which resulted in the absence of a band gap for the 6-QL-thick film. It should be noted that our results for the Bi_2Se_3 film that does not contain basal twins are in good agreement with those previously reported [30–32]. To evaluate possible changes in the surface states in the presence of basal twins, the distributions of the surface states were calculated at two different k-points ((0, 0.050, 0) along the Γ-M line and (0.026,0.053,0) along the K-Γ line) for all four cases discussed above, and the results are presented in Fig. 2(e-h) (bottom). As can be seen, the surface states are quite robust and are only slightly affected by the presence of a basal twin in the film.

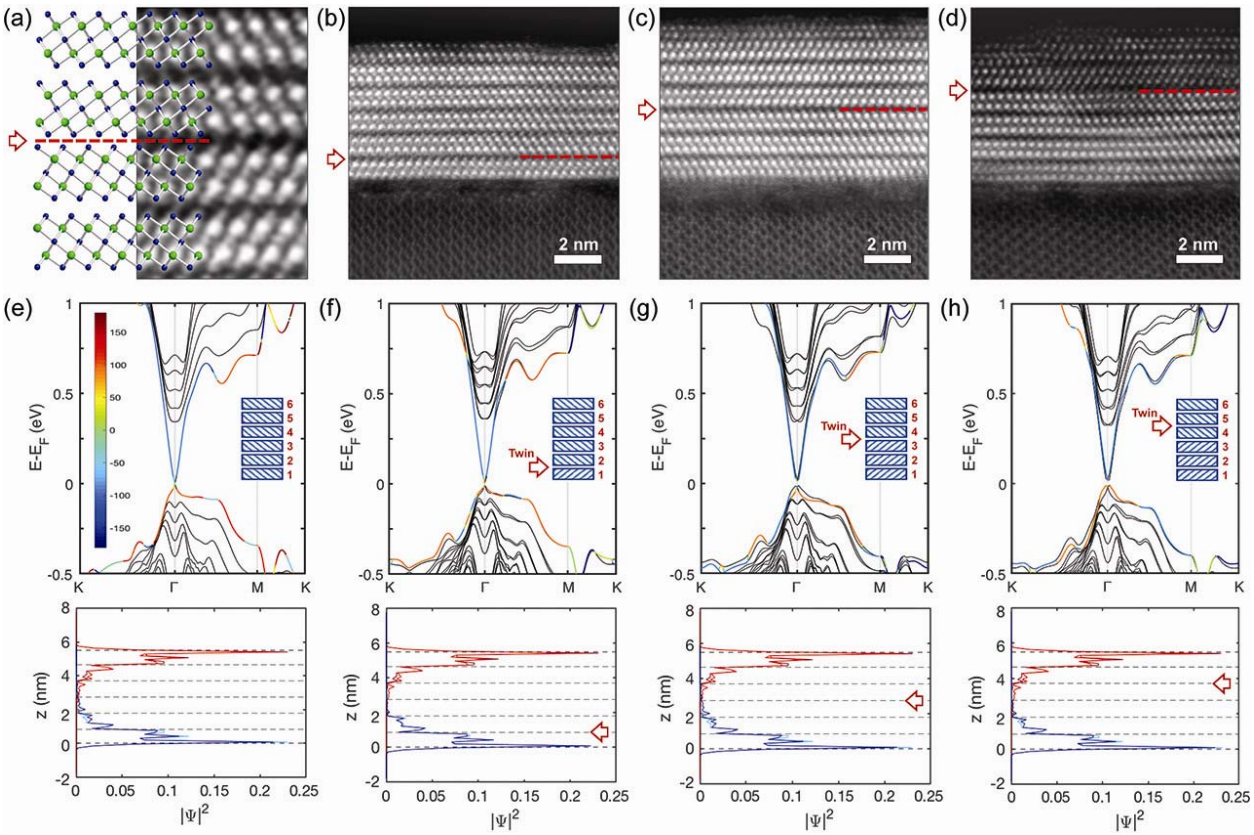

FIG. 2. (a) A model and atomic-resolution HAADF-STEM image of a Bi_2Se_3 basal twin showing the details of the atomic arrangement of the twin. (b-d) Atomic-resolution HAADF-STEM images showing twinning after the first, third, and fourth QLs above the substrate, respectively. (e-h) Electronic band structures (top) and spatial distributions of the surface states across the thickness (bottom, QLs are highlighted with dash lines) of 6-QL-thick pristine and basal twinned Bi_2Se_3 films, as calculated by DFT. The location of the basal twin is indicated in the inset schematic in each case. In these calculations, the lattice parameters for the Bi_2Se_3 thin film were a = 4.11 Å and c = 54.93 Å. The angle between the wavevector and spin of the electron located in the top surface QL is identified by color map.

The exact size of the band gap created due to basal twinning appears to be sensitive to the number of QLs in the film and the location of the twin in the film. The results of calculations performed for different thicknesses of the film and for different locations of the basal twin are presented in Fig. 3(a). Here, the in-plane lattice parameter for all Bi_2Se_3 thin films was kept at a = 4.11 Å, and the height of each QL was fixed at 7.18 Å with an inter-QL distance of 2.37 Å. The kinetic energy cutoff for the plane-wave expansion was set as 300 eV in all calculations, and vacuum thicknesses of 30 Å (or larger) were used to avoid interaction between the adjacent supercells. The energy convergence value was chosen as 10^{-5} eV, and for the structural relaxations, the maximum Hellmann-Feynman force acting on each atom was less than 1 meV/Å. Additional calculations performed for the Bi_2Se_3 thin films (up to 6-QL-thick) using the

optimized out-of-plane lattice parameters from structural relaxation (see Table I) produced very similar results (see Fig. 3(b)), suggesting that the band gap increase in Bi_2Se_3 thin films containing a basal twin can be expected not only for slightly constrained films, but also for free-standing (or relaxed) films. Overall, the effects of the basal twin on the electronic band structure of Bi_2Se_3 thin films have many similarities with those due to changes in the number of QLs in the film [33].

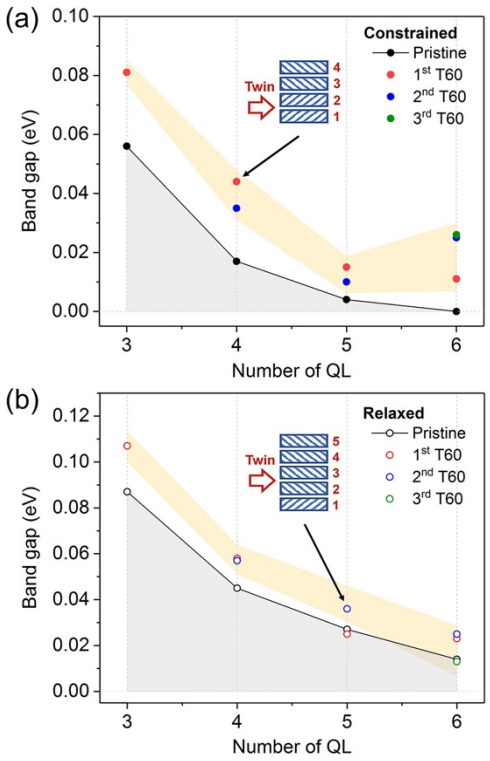

FIG. 3. (a) The band gaps of Bi_2Se_3 films, dominated by the surface states, as a function of film thickness calculated for the pristine and basal twinned (60° twist: T60) films. In these calculations, the in-plane lattice parameter is a = 4.11 Å, and the height of the QLs was fixed at 7.18 Å with an inter-QL distance of 2.37 Å. Examples of film models with a basal twin are shown in the inset. (b) The band gaps of Bi_2Se_3 films as a function of film thickness for the pristine and basal twinned films calculated after relaxing the structures. The lattice parameters, heights of the QLs, and inter-QL distances are listed in Table 1. Yellow shaded regions are guides to the eye.

TABLE 1. Calculated structural parameters for 3-QL to 6-QL relaxed Bi_2Se_3 films: heights of each QL and inter-QL distances. The optimized in-plane lattice constant is a = 4.12 Å for all cases, except for the 5-QL, 1st T60 and 6-QL, 2nd T60 films, for which a = 4.11Å. The calculated bulk height and inter-QL distance are 6.99 Å and 2.66 Å, respectively, similar to other reported values [30].

Structure	Heights of each QL and inter-QL distances. All in Å										
	1st	inter-QL	2nd	inter-QL	3rd	inter-QL	4th	inter-QL	5th	inter-QL	6th
3-QL											
pristine	7.01	2.67	7.00	2.67	7.01						
1st T60	7.02	2.68	7.01	2.73	7.02						
4-QL											
pristine	7.01	2.68	7.01	2.66	7.01	2.68	7.01				
1st T60	7.02	2.68	7.00	2.66	7.00	2.73	7.01				
2nd T60	7.01	2.68	7.01	2.74	7.00	2.67	7.01				
5-QL											
pristine	7.01	2.68	7.00	2.66	6.99	2.66	7.00	2.68	7.01		
1st T60	7.02	2.69	7.00	2.67	7.0	2.66	7.00	2.73	7.02		
2nd T60	7.01	2.68	7.00	2.66	7.00	2.73	7.00	2.67	7.01		
6-QL											
pristine	7.01	2.68	7.00	2.66	6.99	2.66	6.99	2.66	6.99	2.68	7.01
1st T60	7.01	2.69	7.00	2.67	7.00	2.67	7.00	2.65	7.00	2.73	7.01
2nd T60	7.01	2.69	7.00	2.67	7.00	2.66	6.99	2.72	7.00	2.67	7.01
3rd T60	7.01	2.68	7.00	2.66	7.00	2.72	6.99	2.66	7.00	2.68	7.01

The structural characterization presented here shows that the Bi_2Se_3 films grown by MBE onto YIG are more disordered than similar films grown by MBE onto other substrates. There are two main reasons for this. First, AFM and HAADF-STEM measurements show that the YIG film does not have a well-defined, atomically-smooth crystalline surface to template the Bi_2Se_3 growth, although the YIG layer is a uniform single crystal. The cross-sectional HAADF-STEM analysis indicates that the small undulations on the YIG surface result in shallow pits that become infilled with an amorphous metal oxide layer before crystalline Bi_2Se_3 can grow. In some cases, this amorphous layer has small amounts of order in it that exist as an array of heavy atoms concentrated directly below the first QL. Second, these Bi_2Se_3 films contain basal twins at various depths. DFT calculations performed for constrained and relaxed films suggest that the basal twins observed in our STEM experiments will affect the band structure of the film, resulting in further opening of the band gap. The calculations also suggest that the amount of increase in the band gap will depend on the level of strain in the film, thickness of the film, and the location of the twin. Altogether, these results provide important insights that can enable advances in the quality of the YIG substrate and the details of the MBE growth. As a result, it will become possible to minimize structural defects that occur in the Bi_2Se_3 film and to avoid undesirable changes in the electronic structure of the film due to basal twins.

Acknowledgments

This work is supported in part by SMART, one of seven centers of nCORE, a Semiconductor Research Corporation program, sponsored by National Institute of Standards and Technology (NIST). This work

utilized the College of Science and Engineering (CSE) Characterization Facility, University of Minnesota (UMN), supported in part by the NSF through the UMN MRSEC program (No. DMR-1420013); and the CSE Minnesota Nano Center, UMN, supported in part by NSF through the NNIN program. The work at CSU was also supported by NSF (EFMA-1641989) and the Department of Energy (DE-SC0018994). We also acknowledge computational support from the Minnesota Supercomputing Institute (MSI).

References

[1] Y. L. Chen, J. G. Analytis, J.-H. Chu, Z. K. Liu, S.-K. Mo, X. L. Qi, H. J. Zhang, D. H. Lu, X. Dai, Z. Fang, *et al*., Experimental realization of a three-dimensional topological insulator, Bi_2Te_3, Science **325**, 178 (2009).

[2] A. R. Mellnik, J. S. Lee, A. Richardella, J. L. Grab, P. J. Mintun, M. H. Fischer, A. Vaezi, A. Manchon, E.-A. Kim, N. Samarth *et al*., Spin–transfer torque generated by a topological insulator, Nature **511**, 449 (2014).

[3] J. S. Lee, A. Richardella, D. Reifsnyder Hickey, K. A. Mkhoyan, and N. Samarth, Mapping the chemical potential dependence of current-induced spin polarization in a topological insulator, Phys. Rev. B **92**, 155312 (2015).

[4] M. Lang, M. Montazeri, M. C. Onbasli, X. Kou, Y. Fan, P. Upadhyaya, K. Yao, F. Liu, Y. Jiang, W. Jiang, *et al*., Proximity induced high-temperature magnetic order in topological insulator – ferrimagnetic insulator heterostructure, Nano Lett. **14**, 3459 (2014).

[5] H. Wang, J. Kally, J. S. Lee, T. Liu, H. Chang, D. Reifsnyder Hickey, K. A. Mkhoyan, M. Wu, A. Richardella, and N. Samarth, Surface-state-dominated spin-charge current conversion in topological-insulator–ferromagnetic-insulator heterostructures, Phys. Rev. Lett. **117**, 076601 (2016).

[6] Y. T. Fanchiang, K. H. M. Chen, C. C. Tseng, C. C. Chen, C. K. Cheng, S. R. Yang, C. N. Wu, S. F. Lee, M. Hong, and J. Kwo, Strongly exchange-coupled and surface-state-modulated magnetization dynamics in Bi_2Se_3/yttrium iron garnet heterostructures, Nat. Commun. **9**, 223 (2018).

[7] H. Chang, P. Li, W. Zhang, T. Liu, A. Hoffmann, L. Deng, and M. Wu, Nanometer-thick yttrium iron garnet films with extremely low damping, IEEE Magn. Lett. **5**, 6700104 (2014).

[8] A. Richardella, A. Kandala, J. S. Lee, and N. Samarth, Characterizing the structure of topological insulator thin films, APL Mater. **3**, 083303 (2015).

[9] I. Levy, T. A. Garcia, S. Shafique, and M. C. Tamargo, Reduced twinning and surface roughness of Bi_2Se_3 and Bi_2Te_3 layers grown by molecular beam epitaxy on sapphire substrates, J. Vac. Sci. Technol. B, **36**, 02D107 (2018).

[10] L. Seixas, L. B. Abdalla, T. M. Schmidt, A. Fazzio, and R. H. Miwa, Topological states ruled by stacking faults in Bi_2Se_3 and Bi_2Te_3, J. Appl. Phys. **113**, 023705 (2013).

[11] K.-C. Kim, J. Lee, B. K. Kim, W. Y. Choi, H. J. Chang, S. O. Won, B. Kwon, S. K. Kim, D.-B. Hyun, H. J. Kim, *et al*., Free-electron creation at the 60° twin boundary in Bi_2Te_3, Nat. Commun. **7**, 12449 (2016).

[12] Y. Liu, Y. Y. Li, S. Rajput, D. Gilks, L. Lari, P. L. Galindo, M. Weinert, V. K. Lazarov, and L. Li, Tuning Dirac states by strain in the topological insulator Bi_2Se_3, Nat. Phys. **10**, 294 (2014).

[13] S. Borisova, J. Krumrain, M. Luysberg, G. Mussler, and D. Grützmacher, Mode of growth of ultrathin topological insulator Bi_2Te_3 films on Si (111) substrates, Cryst. Growth Des. **12**, 6098 (2012).

[14] S. Borisova, J. Kampmeier, M. Luysberg, G. Mussler, and D. Gru□tzmacher, Domain formation due to surface steps in topological insulator Bi_2Te_3 thin films grown on Si (111) by molecular beam epitaxy, Appl. Phys. Lett. **103**, 081902 (2013).

[15] M. Jamali, J. S. Lee, J. S. Jeong, F. Mahfouzi, Y. Lv, Z. Zhao, B. K. Nikolić, K. A. Mkhoyan, N. Samarth, and J.-P. Wang, Giant spin pumping and inverse spin Hall effect in the presence of surface and bulk spin−orbit coupling of topological insulator Bi_2Se_3, Nano Lett. **15**, 7126 (2015).

[16] A. Richardella, D. M. Zhang, J. S. Lee, A. Koser, D. W. Rench, A. L. Yeats, B. B. Buckley, D. D. Awschalom, and N. Samarth, Coherent heteroepitaxy of Bi_2Se_3 on GaAs (111)B, Appl. Phys. Lett. **97**, 262104 (2010).

[17] C.-L. Song, Y.-L. Wang, Y.-P. Jiang, Y. Zhang, C.-Z. Chang, L. Wang, K. He, X. Chen, J.-F. Jia, Y. Wang, *et al*., Topological insulator Bi_2Se_3 thin films grown on double-layer graphene by molecular beam epitaxy, Appl. Phys. Lett. **97**, 143118 (2010).

[18] B. Li, X. Guo, W. Ho, and M. Xie, Strain in epitaxial Bi_2Se_3 grown on GaN and graphene substrates: A reflection high-energy electron diffraction study, Appl. Phys. Lett. **107**, 081604 (2015).

[19] J. Y. Park, G.-H. Lee, J. Jo, A. K. Cheng, H. Yoon, K. Watanabe, T. Taniguchi, M. Kim, P. Kim, and G.-C. Yi, Molecular beam epitaxial growth and electronic transport properties of high quality topological insulator Bi_2Se_3 thin films on hexagonal boron nitride, 2D Mater. **3**, 035029 (2016).

[20] D. Reifsnyder Hickey, R. J. Wu, J. S. Lee, J. G. Azadani, R. Grassi, M. DC, J.-P. Wang, T. Low, N. Samarth, and K. A. Mkhoyan, Large-scale defects hidden inside a topological insulator grown onto a 2D substrate, arXiv:1808.03719.

[21] P. E. Blöchl, Projector augmented-wave method, Phys. Rev. B **50**, 17953 (1994).

[22] G. Kresse and J. Furthmüller, Efficient iterative schemes for *ab initio* total-energy calculations

using a plane-wave basis set, Phys. Rev. B **54**, 11169 (1996).

[23] J. P. Perdew, K. Burke, and M. Ernzerhof, Generalized gradient approximation made simple, Phys. Rev. Lett. **77**, 3865 (1996).

[24] S. Grimme, Semiempirical GGA-type density functional constructed with a long-range dispersion correction, J. Comput. Chem. **27**, 1787 (2006).

[25] N. V. Tarakina, S. Schreyeck, T. Borzenko, C. Schumacher, G. Karczewski, K. Brunner, C. Gould, H. Buhmann, and L. W. Molenkamp, Comparative study of the microstructure of Bi_2Se_3 thin films grown on Si(111) and InP(111) substrates, Cryst. Growth Des. **12**, 1913 (2012).

[26] L. He, X. Kou, and K. L. Wang, Review of 3D topological insulator thin-film growth by molecular beam epitaxy and potential applications, Phys. Status Solidi RRL **7**, 50 (2013).

[27] N. V. Tarakina, S. Schreyeck, M. Luysberg, S. Grauer, C. Schumacher, G. Karczewski, K. Brunner, C. Gould, H. Buhmann, R. E. Dunin-Borkowski, *et al*., Suppressing twin formation in Bi_2Se_3 thin films, Adv. Mater. Interfaces **1**, 1400134 (2014).

[28] M. DC, R. Grassi, J.-Y. Chen, M. Jamali, D. Reifsnyder Hickey, D. Zhang, Z. Zhao, H. Li, P. Quarterman, Y. Lv, *et al*., Room-temperature high spin–orbit torque due to quantum confinement in sputtered $Bi_xSe_{(1-x)}$ films, Nat. Mater. **17**, 800 (2018).

[29] Y. F. Lee, R. Kumar, F. Hunte, J. Narayan, and J. Schwartz, Control of intrinsic defects and magnetotransport properties of Bi_2Se_3/c-sapphire epitaxial heterostructures, Acta Mater. **95**, 57 (2015).

[30] W. Liu, X. Peng, X. Wei, H. Yang, G. M. Stocks, and J. Zhong, Surface and substrate induced effects on thin films of the topological insulators Bi_2Se_3 and Bi_2Te_3, Phys. Rev. B **87**, 205315 (2013).

[31] O. V. Yazyev, J. E. Moore, and S. G. Louie, Spin polarization and transport of surface states in the topological insulators Bi_2Se_3 and Bi_2Te_3 from first principles, Phys. Rev. Lett. **105,** 266806 (2010).

[32] P. Larson, V. A. Greanya, W. C. Tonjes, R. Liu, S. D. Mahanti, and C. G. Olson, Electronic structure of Bi_2X_3 (X = S, Se, Te) compounds: Comparison of theoretical calculations with photoemission studies, Phys. Rev. B **65**, 085108 (2002).

[33] Y. Zhang, K. He, C.-Z. Chang, C.-L. Song, L.-L. Wang, X. Chen, J.-F. Jia, Z. Fang, X. Dai, W.-Y. Shan, *et al*., Crossover of the three-dimensional topological insulator Bi_2Se_3 to the two-dimensional limit, Nat. Phys. **6**, 584 (2010).